

Hole relaxation in p -type $\text{In}_x\text{Ga}_{1-x}\text{As}/\text{Al}_y\text{Ga}_{1-y}\text{As}$ quantum wells observed by ultrafast midinfrared spectroscopy

Z. Xu and P. M. Fauchet

Department of Electrical Engineering, University of Rochester, Rochester, New York 14627

C. W. Rella, B. A. Richman, and H. A. Schwettman

Stanford Picosecond FEL Center, W. W. Hansen Experimental Physics Laboratory, Stanford University, Stanford, California 94305

G. W. Wicks

The Institute of Optics, University of Rochester, Rochester, New York 14627

(Received 24 October 1994; revised manuscript received 28 December 1994)

We have performed midinfrared pump-probe transmission measurements in p -type strained $\text{In}_{0.5}\text{Ga}_{0.5}\text{As}/\text{Al}_{0.5}\text{Ga}_{0.5}\text{As}$ quantum wells at room temperature. The laser source was a midinfrared free-electron laser generating subpicosecond pulses and tuned on resonance between the heavy-hole and the light-hole subbands. The relaxation time is ~ 1 ps, which is shorter than for electrons in the conduction band. Interactions between the optical phonons and holes account for the measured relaxation.

The mechanism of intersubband relaxation in quantum wells (QW's) is very important from a fundamental physics perspective and for device applications. Recent measurements performed by infrared bleaching techniques in n -type QW's have revealed a relaxation time ranging from 1 to 10 ps when the well is narrow enough to make the intersubband transition energy larger than the LO-phonon energy, so that electron-LO-phonon scattering is allowed.¹⁻³ These relaxation times are longer than the theoretical predictions.⁴ This discrepancy is believed to result from the complexity of the band structure and experimental conditions, such as the combined effects of LO-phonon screening, intervalley scattering, and hot phonons.⁵ Subpicosecond time-resolved anti-Stokes Raman-scattering measurements give an intersubband relaxation time of less than 1 ps when a very low excitation intensity was employed.⁶ For p -type quantum wells, the density of states and the band structure are different, and it would be interesting to determine the roles of different scattering mechanisms, such as LO-phonon scattering and the optical deformation-potential scattering. A determination of the cooling rate for holes performed by time-resolved photoluminescence yielded a relaxation time of 1 ps.⁷ However, these measurements are not direct since both electrons and holes were present. A direct determination requires that no electrons be photo-generated. Free-electron lasers can generate infrared pulses and are suitable for pump-probe experiments.⁸ In this paper, we report a direct measurement of the relaxation time of holes in p -type quantum wells by the pump-probe technique using < 1 -ps pulses generated by a midinfrared free-electron laser.

The samples used in our experiments were strained quantum wells grown by molecular-beam epitaxy (MBE). Because of the significant lattice mismatch between $\text{In}_x\text{Ga}_{1-x}\text{As}$ and $\text{Al}_x\text{Ga}_{1-x}\text{As}$, a $2\text{-}\mu\text{m}$ -thick buffer layer, in which the indium concentration varied linearly from 0 to 30%, was grown between the QW layer and the GaAs substrate in order to obtain high quality samples.⁹

The substrate temperature during the growth of the quantum wells was between 450 and 525°C. The QW layer consists of 50 $\text{In}_{0.5}\text{Ga}_{0.5}\text{As}/\text{Al}_{0.5}\text{Ga}_{0.5}\text{As}$ periods. The $\text{In}_{0.5}\text{Ga}_{0.5}\text{As}$ well was 4 nm wide, and the $\text{Al}_{0.5}\text{Ga}_{0.5}\text{As}$ barrier was 8 nm wide. Thin 5.7-Å-thick GaAs smooth layers were added at the interfaces for optimal growth.⁹ Two samples were grown: one in which the whole quantum-well layer was doped by Be, and another one which was undoped to provide a good reference in the linear absorption measurement. The dopant concentration is 10^{19} cm^{-3} , and the sheet density is thus $1.2 \times 10^{13}\text{ cm}^{-2}$ if the carriers are all transferred to the wells.

The room-temperature Fourier transform infrared (FTIR) spectrum is shown in Fig. 1. The signal for the undoped sample was used as the reference. As a result the etalon effects from the epitaxial layer could be elim-

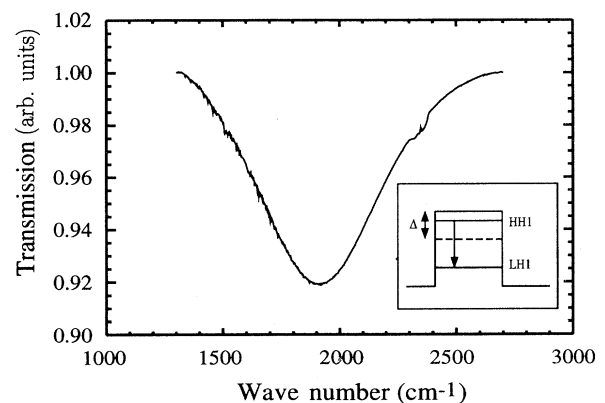


FIG. 1. Infrared absorption of the QW sample. The strong absorption is due to the heavy-hole 1 to light-hole 1 transition as indicated in the inset. Δ is the strain-induced energy splitting.

inated and a clean absorption spectrum was obtained.¹⁰ An absorption peak was observed at $5.25 \mu\text{m}$ (220 meV) with a full width at half maximum (FWHM) of 50 meV. We attribute the absorption peak of Fig. 1 to the heavy-hole 1 (HH1) to light-hole 1 (LH1) transition as indicated in the inset. A simple effective-mass approximation model was used to estimate the absorption peak position. The strain-induced energy splitting between the heavy-hole state and the light-hole states is $\Delta = 150 \text{ meV}$,¹¹ while the quantum-confinement-induced energy splitting is 90 meV at $\mathbf{k} = 0$. As a result the total-energy difference between the heavy- and light-hole states is estimated to be 240 meV, which is consistent with what we observed in the absorption spectrum (220 meV). The absorption peak is very wide compared to that in n -type quantum wells, where typically the peak width is a few meV.¹⁰ The hole gas in our sample is highly degenerate because of the high doping level and the small in-plane effective mass of the heavy-hole bands. Since the effective masses in the HH1 and LH1 bands are quite different, the absorption spectrum is expected to be very broad. State broadening due to hole-hole scattering can also contribute to the width of the absorption peak.¹² We cannot exclude that inhomogeneities introduced during growth, i.e., fluctuations of the well width and possible relaxation of the strain, may play a secondary role. From our calculation, there is also another state (heavy hole 2), which is located approximately 100 meV away from HH1. We cannot resolve this transition in our FTIR spectrum because the Fermi energy is below the HH2 subband edge.¹³ The existence of this state provides another channel of relaxation, which increases the rate at which the holes can be scattered from the LH1 subband.

We performed equal-wavelength pump-probe measurements at room temperature near $5 \mu\text{m}$. We used the Stanford picosecond free-electron laser (FEL) as the laser source. The output of the FEL was a macropulse train with a repetition rate of either 10 or 20 Hz and a macropulse duration of 3 ms. Each macropulse was made of a micropulse train with individual pulses separated by 85 ns and of a duration that is less than 1 ps. The laser was tunable from 4 to $6 \mu\text{m}$. A single-pulse selection technique was used to reduce the thermal effects during the experiments. The pump and probe were focused to a spot size of $\sim 50 \mu\text{m}$. The peak intensity of the pump pulse on the sample was varied from 0.1 to $10 \text{ GW}/\text{cm}^2$. The ratio of the intensities of the probe pulse and the pump pulse on the sample was less than 1:5. The transmitted probe light was detected by a fast detector. The difference between the transmission of the sample with and without the pump was measured as a function of the delay time between the pump and the probe pulses.

The change of transmission measured at $5.05 \mu\text{m}$ with a pump intensity of $1.5 \text{ GW}/\text{cm}^2$ is shown in Fig. 2 on a linear scale. For the analysis of the data, we assumed a two-level system and used the population equations as described in Ref. 14:

$$\frac{dN_2}{dt} = \frac{\sigma I(t)}{h\nu} (N_1 - N_2) - \frac{N_2}{\tau}, \quad (1)$$

where N_1 is the population in the ground state, N_2 is the

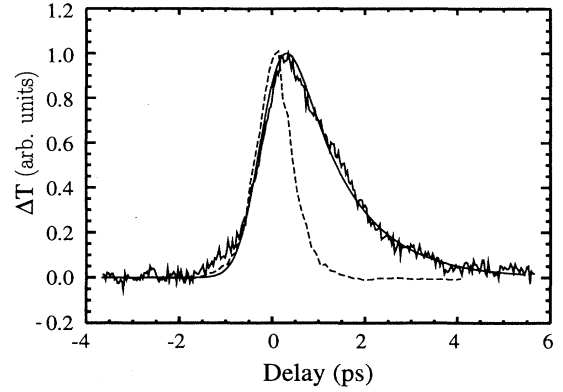


FIG. 2. Pump-induced transmission change of the probe beam for a pump intensity of $1.5 \text{ GW}/\text{cm}^2$ measured at $5.05 \mu\text{m}$ as a function of the delay time, on a linear scale. The solid line is the best fit using an exponential relaxation with $\tau = 1.1 \text{ ps}$. The dashed line is the autocorrelation signal.

population in the excited state, σ is the absorption cross section, and τ is the relaxation time. The induced transmission change ΔT in the probe is

$$\Delta T \propto \int_{-\infty}^{\infty} I(t - t_D) (N_1 - N_2) dt, \quad (2)$$

where t_D is the delay time between the pump pulse and the probe pulse. The above equations were solved numerically and fit to the experimental data to extract the relaxation time τ . The solid line in Fig. 2 corresponds to a relaxation time $\tau = 1.1 \text{ ps}$ and is the best fit. The dashed line is the pulse autocorrelation. It has a Gaussian shape and the pulse duration is 0.7 ps. It must be noted that, in this simple fit, the spatial profile of the beams was not taken into account, which puts a limit on the accuracy of the relaxation time we extracted.

In Fig. 3, we plot the same data on a logarithmic scale, together with theoretical curves calculated using $\tau = 0.5, 1.1, \text{ and } 1.5 \text{ ps}$, to show our ability to extract with precision a relaxation time slightly longer than the pulse duration. We also measured the signal at different excita-

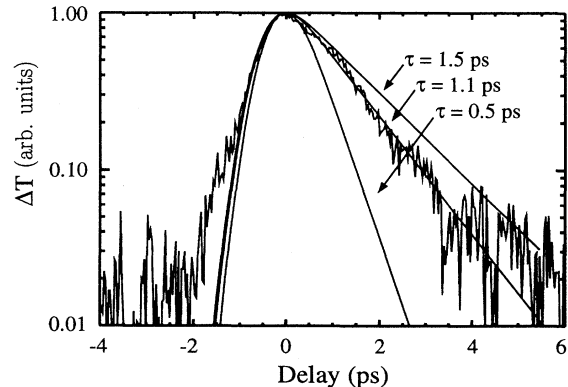


FIG. 3. Pump-induced transmission change of the probe beam for a pump intensity of $1.5 \text{ GW}/\text{cm}^2$ measured at $5.05 \mu\text{m}$ as a function of the delay time, on a logarithmic scale. The fits assumed an exponential relaxation with $\tau = 0.5, 1.1, \text{ and } 1.5 \text{ ps}$.

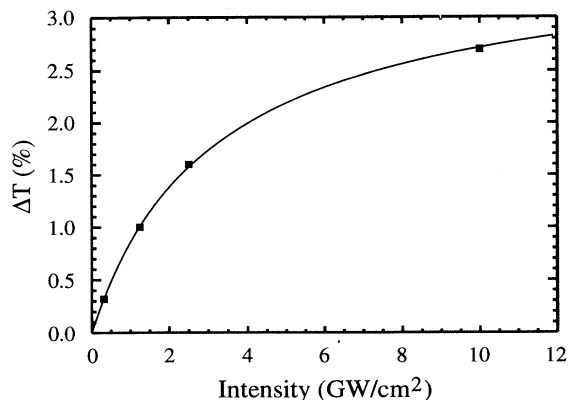


FIG. 4. Peak value of the pump-induced transmission change of the probe beam as a function of pump intensity at $5.05 \mu\text{m}$. The solid line corresponds to the best fit with a saturation intensity of $3 \text{ GW}/\text{cm}^2$ and a complete bleaching $\Delta T(I \rightarrow \infty) = 3.6\%$.

tion intensities. Figure 4 shows the maximum induced transmission as a function of the relative intensity. The solid line is a best fit assuming a homogeneously broadened two-level system. The saturation intensity obtained in this way is $3 \text{ GW}/\text{cm}^2$. The complete bleaching is $\Delta T(I \rightarrow \infty) = 3.6\%$. This saturation intensity is significantly higher than that in *n*-type quantum wells.¹ There are at least two reasons for this difference. First, the absorption cross section for our *p*-type sample is much smaller (by about one order of magnitude) than that for *n*-type quantum wells. Second, the saturation intensity measured here is not exactly the saturation intensity for a two-level system but rather the intensity necessary to draw all of the carriers out of the two-level system. This is shown more clearly below. The data in Figs. 2 and 3 were taken to at pump intensity of $1.5 \text{ GW}/\text{cm}^2$. We also performed pump-probe measurements as a function of pump intensity. The relaxation time increases with increasing intensity, but in all cases it remains well below 2 ps. Figure 5 shows relaxation times at different excitation intensities. The data clearly show a trend to-

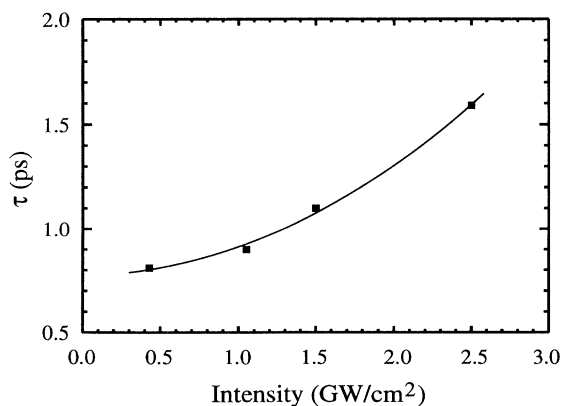


FIG. 5. Relaxation time as a function of pump intensity at $5.05 \mu\text{m}$. The solid line is a guide to the eye.

ward increasing relaxation times with increasing excitation intensity. Finally we tuned the laser in the absorption band from 4.75 to $5.26 \mu\text{m}$. As is expected from a homogeneously broadened system, the relaxation time appeared to be wavelength independent within the accuracy of our measurements.

In order to explain our experimental results, we performed calculations for both LO-phonon scattering and optical deformation-potential scattering in the way indicated in Refs. 4 and 15. A guided mode model is used to describe the phonons.¹⁵ The matrix element for the scattering process is proportional to $I^2(\mathbf{k}, \mathbf{k}')$, where \mathbf{k} and \mathbf{k}' are the wave vectors of the initial and final states, respectively, and $I^2(\mathbf{k}, \mathbf{k}')$ is the overlap term, which is equal to $(1 + 3 \cos^2 \theta_k)/4$ for intrasubband scattering, and is equal to $3/4 \sin^2 \theta_k$ for intersubband scattering, where θ_k is defined as the angle between \mathbf{k} and \mathbf{k}' .¹⁶ We simply assume a parabolic band structure and ignore the mixing between heavy-hole and light-hole bands resulting from quantum confinement effects. Screening is included as given by Asada.¹² The screening length is calculated assuming a completely degenerate hole gas. At room temperature scattering with photons is mainly through emission. The calculations show that the LO-phonon-scattering rate is smaller than the optical deformation-potential scattering rate for both intersubband (LH1-HH1 and LH1-HH2) and intrasubband (HH1-HH1) scattering. The LH1-HH1 scattering rate due to deformation potential scattering with screening is approximately 0.5 ps^{-1} . It is smaller than the intrasubband scattering rate by a factor of 2, and is significantly smaller than that obtained by others with a larger effective mass.¹⁷ The LH1-HH2 scattering rate is approximately 1 ps^{-1} . Thus the total rate at which the holes are scattered away from the excited subband (LH1) is 1.5 ps^{-1} . The HH2-HH1 scattering rate is approximately 2 ps^{-1} , which is faster than all the other scattering processes mentioned above.

Using these considerations as a guide, we can draw a schematic diagram of the scattering processes as shown in Fig. 6. The holes in the excited subband (LH1) relax to

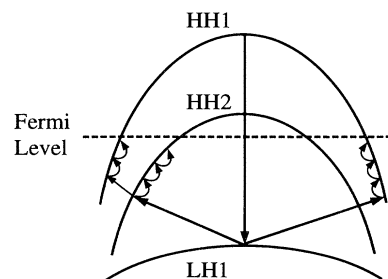


FIG. 6. Schematic diagram of the absorption and scattering processes between two subbands in k_{\parallel} space. The carriers are excited to the upper subband (LH1) by the pump beam, and scatter to the lower band through LO-phonon scattering through two channels: LH1-HH1 and LH1-HH2-HH1, are then thermalized by hole-hole scattering, and finally cool down through optical- and acoustic-phonon emission.

the ground state (HH1) by two different routes. The first is when they are scattered directly to the HH1 subband. The second is when the holes relax in two steps, first to the HH2 subband and then to the HH1 subband. In both cases, relaxations are accomplished mainly by optical phonon emission on a time scale of 1 ps or less. Subsequently, the hot holes in the HH1 subband cool down. This step is more complicated since hole-hole scattering can cool the hot holes by transferring energy to the cold hole reservoir. This process is very efficient due to the high degeneracy of the hole gas in our sample. However, it is generally very fast¹⁸ and is out of reach of our picosecond time resolution experiments. This suggests that the relaxation observed in our experiments is mainly due to intersubband scattering. The relaxation time of ~ 0.6 ps calculated using our simple model is comparable to the relaxation time we observed. Careful theoretical treatments will be needed to provide a more quantitative comparison with our experimental results. Finally, the in-

crease of the relaxation time as the excitation intensity increases is probably not due to the hot phonons,¹⁹ because they would increase the initial scattering rate. The increase of the relaxation time may be caused by the fact that at high injection levels, the ground state stays depleted for a longer time.

In conclusion, we report a measurement of the intravalence band relaxation in *p*-type quantum wells by the infrared bleaching technique. Relaxation times in the 1-ps range were observed. We attribute this relaxation time to the intersubband scattering with optical phonons.

Z.X., P.M.F., and G.W.W. acknowledge the support of the U.S. Office of Naval Research through Contract N00014-92-J-4063, and C.W.R., B.A.R., and H.A.S. acknowledge the support of the U.S. Office of Naval Research through Contract N00014-91-C-0170. We would like to thank M. W. Koch for the growth of the samples.

¹A. Seilmeier, H.-J. Hubner, G. Abstreiter, G. Weimann, and W. Schlapp, *Phys. Rev. Lett.* **59**, 1345 (1987).

²F. H. Julien, J.-M. Lourtioz, N. Herschkorn, D. Delacourt, J. P. Pocholle, M. Papuchon, R. Planel, and G. Le Roux, *Appl. Phys. Lett.* **53**, 116 (1988).

³T. Elsaesser, R. J. Bauerle, W. Kaiser, H. Lobentanzer, W. Stolz, and K. Ploog, *Appl. Phys. Lett.* **45**, 256 (1989).

⁴B. K. Ridley, *Phys. Rev. B* **39**, 5282 (1989).

⁵F. F. Sizov and A. A. Rogalski, *Prog. Quantum Electron.* **17**, 93 (1993).

⁶M. C. Tatham, J. R. Ryan, and C. T. Foxon, *Phys. Rev. Lett.* **63**, 1637 (1989).

⁷J. N. Sweetser, T. J. Dunn, L. Waxer, I. A. Walmsley, S. M. Shank, and G. W. Wicks, *Appl. Phys. Lett.* **63**, 3461 (1993).

⁸P. M. Fauchet, D. A. Young, W. L. Wighan, Jr., and C. M. Fortmann, *IEEE J. Quantum Electron.* **QE-27**, 2714 (1991).

⁹H. C. Chui, E. L. Martinet, M. M. Fejer, and J. S. Harris, Jr.,

Appl. Phys. Lett. **64**, 736 (1994).

¹⁰S.-J. B. Yoo, Ph. D. thesis, Stanford University, 1991.

¹¹X. Z. Lu, R. Garuthara, S. Lee, and R. R. Alfano, *Appl. Phys. Lett.* **52**, 93 (1988).

¹²M. Asada, *IEEE J. Quantum Electron.* **QE-25**, 2019 (1989).

¹³B. J. Vartanian and J. S. Harris, Jr., *SPIE Proc.* **2139**, 27 (1993).

¹⁴B. N. Murdin, G. M. H. Knippels, A. F. G. van der Meer, C. R. Pidgeon, C. J. G. M. Langerak, M. Helm, W. Heiss, K. Unterrainer, E. Gornik, K. K. Geerincck, N. J. Hovenier, and W. Th. Wenckebach, *Semicond. Sci. Technol.* **9**, 1554 (1994).

¹⁵B. K. Ridley, *J. Phys. C* **15**, 5899 (1982).

¹⁶J. D. Wiley, *Phys. Rev. B* **4**, 2485 (1971).

¹⁷S. Seki and K. Yokoyama, *J. Appl. Phys.* **76**, 7399 (1994).

¹⁸J. F. Young, T. Gong, P. M. Fauchet, and P. J. Kelly, *Phys. Rev. B* **50**, 2208 (1994).

¹⁹J. Shah, *IEEE J. Quantum Electron.* **QE-22**, 1728 (1986).